Electrical Power and Energy Systems 146 (2023) 108730

Contents lists available at ScienceDirect

International Journal of Electrical Power and Energy Systems

journal homepage: www.elsevier.com/locate/ijepes

Black-start capability of PV power plants through a grid-forming control based on reactive power synchronization

Andrés Peña Asensio, Santiago Arnaltes Gómez *, Jose Luis Rodriguez-Amenedo

University Carlos III de Madrid, Department of Electrical Engineering, 28911 Leganes, Spain

ARTICLE INFO

Keywords:
Black-start
Islanded operation
Frequency control
Voltage control
Photovoltaic

ABSTRACT

Power system restoration is a critical process for any power system. As synchronous generators are being replaced by power electronic converters used in renewable energy generation, the contribution of renewable energy power plants to power system restoration (PSR) after a black-out is becoming more relevant, the so-called black start capability. Existing solutions for providing black start capability to photovoltaic (PV) power plants rely on the use of energy storage systems (ESS) in a hybrid PV plant. In contrast, this paper proposes a solution for the contribution of PV power plants to the PSR that allows a completely autonomous black start process. Reactive power synchronization is used for controlling the PV inverters as virtual synchronous generators (VSG), providing grid-forming control and ensuring synchronism. During the black start process, the PV power is regulated to match the demand using a decentralized solution to share the load between multiple PV inverters. The solution has been validated to handle the most critical situations during the black start process such as the variation on the power source, i.e. irradiance, or on the supplied load and the connection to the main grid.

1. Introduction

Power system restoration (PSR) has been traditionally carried out by high power generators connected to the transmission system [1]. However, the paradigm of power systems is changing as the share of renewable energy increases. This background leads to an increasing interest of power system operators in the role that renewable energy will have to play on the system operation. In the US, the National Renewable Energy Laboratory (NREL) has highlighted PSR as one of the main challenges of future power systems [2].

The contribution of photovoltaic (PV) plants to the PSR is receiving a growing interest in the literature. In contrast to wind power, the availability of PV generation can be more easily predicted for planning the PSR at a system level. However, most studies have focused on the coordination between PV and conventional generators or energy storage systems (ESSs) [3–7]. Specifically, ESSs can provide the power and energy reserve that allow the hybrid PV plant to perform the load following [8,9].

In contrast, this paper proposes a control system that allows PV plants to contribute to the PSR autonomously, without relying on any additional generator or ESS. This could allow for a significant cost saving in the provision of PSR when there is enough PV resource available. The proposed solution to avoid the use of ESSs during the PSR is based on applying grid-forming control (GFC) to the PV inverters.

GFC can be used to operate PV inverters as voltage sources, instead of constant power sources. As a voltage source, an inverter is able to maintain constant voltage and frequency during islanded operation and also to follow active and reactive power commands when connected to the grid. By maintaining constant voltage and frequency, it is ensured that the GFC supplies the demanded load. In a PV inverter, this demand has to be supplied by the PV generator. However, previous works on GFC rely on the assumption that an ideal dc source is used [10–14]. In [15] it is discussed how a more accurate model of the source connected to the dc side of the inverter could have a significant impact on the GFC operation.

The electrical operation of a PV generator can be represented by its power–voltage, P(V), characteristic curve. P(V) characteristics have been extensively considered in the development of maximum power point tracking (MPPT) strategies such as the incremental conductance [16–18], perturbation and observation [19–21] and other based on fuzzy logic and neural networks [22]. A MPPT strategy regulates the PV generator voltage in order to work at the maximum power for the current irradiance and temperature conditions.

When following a MPPT strategy in grid-connected mode, PV plants can use a GFC. However, since they are operating at their maximum possible power, they will not be able to supply the demanded load.

* Corresponding author.
E-mail addresses: apenaasensio@gmail.com (A. Peña Asensio), arnalte@ing.uc3m.es (S. Arnaltes Gómez), amenedo@ing.uc3m.es (J.L. Rodriguez-Amenedo).

https://doi.org/10.1016/j.ijepes.2022.108730
Received 22 April 2022; Received in revised form 6 October 2022; Accepted 13 October 2022
Available online 4 November 2022
0142-0615/© 2022 The Author(s). Published by Elsevier Ltd. This is an open access article under the CC BY license (http://creativecommons.org/licenses/by/4.0/).

In order to be able to supply the demanded load, either increasing or decreasing the output power, the dc voltage at the PV inverters has to be above the maximum power point voltage. This results in a tradeoff between energy generation and the contribution of PV plants to power regulation. Note that although a voltage below the maximum power value is also possible, it would require a higher current for the same power level, resulting in a lower efficiency, and therefore it is not recommended [23].

A solution to operate PV inverters as grid-forming converters is to use a virtual synchronous generator (VSG) control. VSG solutions have demonstrated their capability to provide GFC [10–14]. Specifically, a VSG is applied for PV generators performing a black-start in [24]. However, VSG implementations use the relationship between power and frequency as synchronizing mechanism [25,26]. Therefore, it is not possible to maintain synchronism if the power required by the synchronizing mechanism cannot be controlled since the power–frequency droop demands a power sharing that cannot be achieved. This is the case in PV plants, where active power depends on available solar irradiance. In contrast to VSG solutions, this paper proposes to use a Reactive Power Synchronization (RPS) method for grid-connected PV inverters. This avoids the dependency of the synchronization on the active power and thus on the resource availability [27,28].

The proposed solution allows PV plants to perform a black-start process and then, after energizing the islanded system, being connected to the main grid to contribute to the PSR. In contrast with previous works, this paper does not assume an ideal power source connected at the dc side of the converter. Instead, a comprehensive model of a PV plant is used to demonstrate the operation of the proposed solution. By using this model, dc voltage variations are obtained as a result of the changes in the demanded power. Provided that enough solar resource is available, it is also demonstrated that the dc voltage is automatically adjusted to the value required for supplying the power demanded by the load. Moreover, the proposed solution allows for the parallel operation of multiple PV inverters, as it is the case on a PV plant. The use of the RPS allows also for the PV inverters synchronization, regulating the terminal voltage and frequency while sharing the demanded load as per the available power. Moreover, it also allows a soft transition to grid-connected mode through the synchronization with another power system. Once the PV plant is connected to the grid, it is possible to modify the active and reactive power, for instance to follow a MPPT strategy or modifying active and reactive power following frequency and voltage deviations, respectively. The control systems required for setting these active and reactive power references would operate on top of the proposed solution. The definition of such control systems is out of the scope of the paper and already covered in previous publications [29], as this paper is focused on the islanded operation required for the contribution to a black-start process.

Next section presents a comprehensive model of two PV inverters connected in parallel in a PV plant that can operate both isolated and connected to the grid. The two inverters case is used to demonstrate how the decentralize nature of the proposed control system allows for the parallel operation of multiple generators. Eigenvalue analysis is used to demonstrate the stability of the controlled system. Then, the capabilities of the proposed solution are validated though a comprehensive simulation to show the operation during a black start process that includes variations in the load and irradiance and also the synchronization to the grid.

2. PV plant model and analysis

This section presents the state-space model of a PV plant composed by two PV generators, as seen in Fig. 1. The model is presented in per-unit (pu) using the base values given in Table 1. Variables in pu are represented in lowercase. The dc base voltage is selected as twice the peak ac phase voltage to simplify the PV inverter model as proposed in [30].

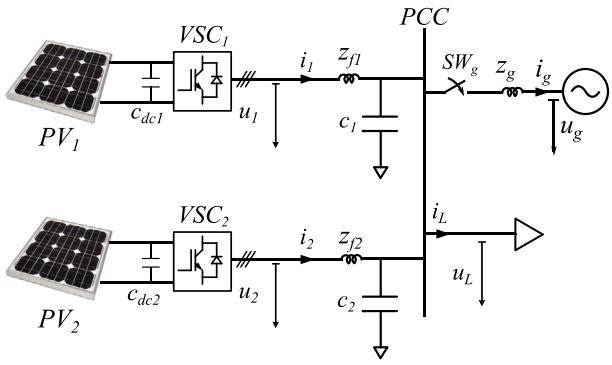

Fig. 1. Schematic representation of the PV power plant case study.

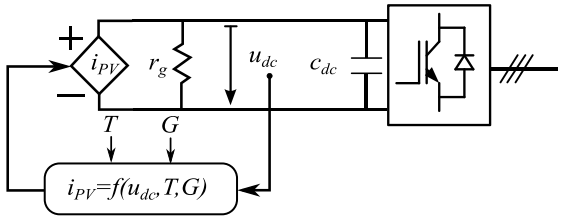

Fig. 2. PV generator equivalent circuit.

Table 1
Base values for per unit transformations.

Label	Value	Units	Description
U_b	$400 * \sqrt{2/3}$	V	Base ac voltage (peak phase voltage)
$U_{dc,b}$	$2U_b$	V	Base dc voltage
S_b	2	MVA	Base power
f_b	50	Hz	Base frequency
Ω_b	$2\pi f_b$	rad/s	Base angular frequency

Following, the model of a PV generator is provided to demonstrate how the proposed solution balances generation and demand in isolated mode. Then, the PV inverters operation in both islanded and grid-connected modes is discussed.

2.1. PV generator

The PV generator model is given by its Norton equivalent, as depicted in Fig. 2. The Norton equivalent current, i_{PV}, and internal resistance, r_g, are defined, following [23], as

$$i_{PV} = N_p i_i \left(\frac{r_p}{r_s + r_p} \right) \tag{1}$$

$$r_g = \frac{N_s}{N_p}(r_s + r_p) \tag{2}$$

where r_s and r_p are the series and parallel resistances of the PV module, respectively. N_s and N_p are the number of modules connected in series forming a string and the number of strings connected in parallel. This allows to extend the model of a single module for the full PV generator, assuming all modules are of the same type and subjected to the same meteorological conditions. Thus, i_i can be defined as the current at a single ideal module terminals by

$$i_i = i_{ph} - i_0 \left[e^{\left(\left(\frac{r_p}{r_s + r_p} \right) \frac{u_{dc} + r_s i_i}{\alpha v_{th}} \right)} - 1 \right] \tag{3}$$

Therefore, the current at the module terminals will depend on i_0, i_{ph}, u_{dc}, α and v_{th} on top of the internal resistances. The current i_0, which is approximately equal to the short-circuit current of the PV module, the ideality factor, α, and the thermal voltage, v_{th}, are characteristic

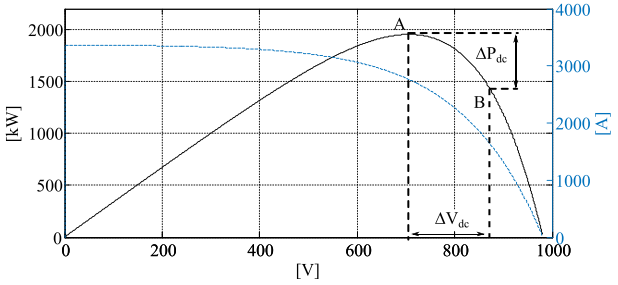

Fig. 3. $I(V)$ and $P(V)$ characteristics curves of a PV generator.

Table 2
PV generator parameters.

Label	Value	Units	Description
$P_{dc,max}$	2000	kW	Maximum power
$V_{dc,max}$	700	V	Maximum power–voltage
V_{oc}	872	V	Open circuit voltage
I_{sc}	3098	A	Short-circuit current
R_s	5.88	Ω	Series resistance
R_p	11	kΩ	Parallel resistance
R_g	29.75	Ω	Norton impedance
C_{dc}	150	mF	Total dc capacitance
N_s	27		Number of modules in series
N_p	370		Number of modules in parallel

parameters of the PV module while i_{ph} is the light-generated or photovoltaic current, and is defined as a function of the irradiance, G(W/m^2), and temperature, T(° C), at the PV module.

The PV generator parameters shown in Table 2 have been used in this paper. Based on these parameters, Fig. 3 shows the $I(V)$ and $P(V)$ characteristics of the PV generator. It can be seen that maximum power, $P_{dc,max} = 2$ MW, is obtained at a voltage of $V_{dc,max} = 700$ V (point A).

2.2. Parallel connected PV inverters model

This section presents the state-space model of two PV inverters operating in parallel, following the scheme shown in Fig. 1. Two cases will be analysed: isolated operation and grid-tied operation, depending on the state of the switch SW_g in Fig. 1.

The ac side of each inverter is modelled as a controllable voltage source u which is represented by its direct and quadrature (dq) components in a rotating reference frame [30]. The rotational frequency is set as an internal value, ω, calculated by the inverter control. The calculation of this internal frequency will be discussed later in the paper. Based on the above, the current at the inverter terminals, i, can be obtained as

$$\frac{l_f}{\Omega_b}\frac{di_d}{dt} = u_d - u_{dL} - r_f i_d + \omega l_f i_q \tag{4}$$

$$\frac{l_f}{\Omega_b}\frac{di_q}{dt} = u_q - u_{qL} - r_f i_q - \omega l_f i_d \tag{5}$$

where u_L is the voltage at the point of common coupling (PCC) and r_f and l_f are the resistive and inductive components of the filter impedance z_f. These equations are the basis of the control of the inverter current, i using the terminal voltage, u.

In the two inverter system of Fig. 1, considering the filter capacitors, c_1 and c_2, the voltage at the PCC can be calculated as a function of the inverter currents, i_1 and i_2, as

$$\left(\frac{c_1 + c_2}{\Omega_b}\right)\frac{du_{dL}}{dt} = i_{d1} + i_{d2} - i_{dg} - i_{dL} + \omega(c_1 + c_2)u_{qL} \tag{6}$$

$$\left(\frac{c_1 + c_2}{\Omega_b}\right)\frac{du_{qL}}{dt} = i_{q1} + i_{q2} - i_{qg} - i_{qL} - \omega(c_1 + c_2)u_{dL} \tag{7}$$

where i_g is the grid current and i_L is the load current.

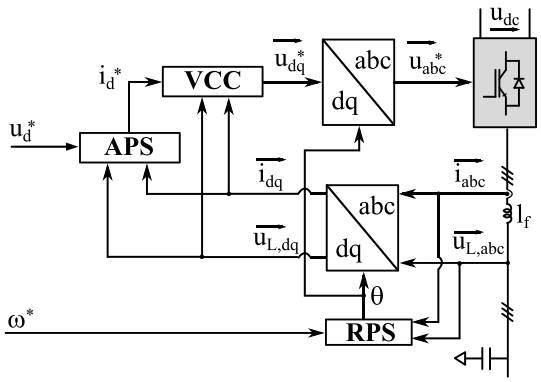

Fig. 4. Voltage Source Converter (VSC) control for parallel operation. RPS: Reactive Power Synchronization, APS: Active Power Sharing, VCC: Voltage and Current Controllers.

From Eq. (6) it follows that the balance of active currents ($i_{d1}+i_{d2} = i_{dg} + i_{dL}$) will be ensured when the voltage magnitude at the PCC is constant ($\frac{du_{dL}}{dt} = 0$). For the black-start process, where $i_{dg} = 0$ (see Fig. 1), this means that if the control is able to regulate a constant voltage magnitude, the PV generators will be supplying the load active power.

A similar reasoning for Eq. (7) leads to ensure that if the control is able to regulate a constant angle between the grid voltage and the internal control reference frame ($\frac{du_{qL}}{dt} = 0$), the PV generators will be supplying the load reactive power during the black-start.

In [27] it is demonstrated how it is possible to regulate the phase displacement between the PCC voltage, $\vec{u_L}$, and the inverter voltage, $\vec{u}$, using the exchanged reactive power. In this paper, the relationship between reactive power and phase displacement will be used to regulate the phase displacement between both PV inverters.

Considering this PV inverter model, if the control is able to ensure a constant voltage magnitude and angle, the PV generators will be able to operate in synchronism with each other while supplying the power demanded by the loads. Moreover, they will also be able to synchronize with the grid.

3. Control system for black-start

Based on the model presented in the previous section, the control system for the black-start of the PV generators is proposed in this section. The main objective of this control system is that the PV generators are able to operate in an isolated system, providing the active and reactive power demanded by the loads.

An important constraint to consider is that in a power converter it is not possible to control the dc voltage and ac voltage at the same time. For the isolated operation during the PSR, the PV inverters have to generate the grid voltage, by controlling the magnitude and frequency of the ac voltage. But, as stated before, during the isolated operation of the PV plant, dc voltage is automatically regulated to the value required to achieve the power balance.

The proposed control system is presented in Fig. 4. It is divided in three blocks, that are explained the following sections, the Voltage and Current Controllers (VCC), the Reactive Power Synchronization (RPS) and the Active Power Sharing (APS).

3.1. Voltage and current controllers

The Voltage and Current Controllers (VCC) are depicted in Fig. 5. This VCC is a common solution for inverter control due to its ability to regulate the inverter current during faults [27].

Using the VCC as given in Fig. 4, by controlling the quadrature component of the generated voltage to zero, it is ensured that the

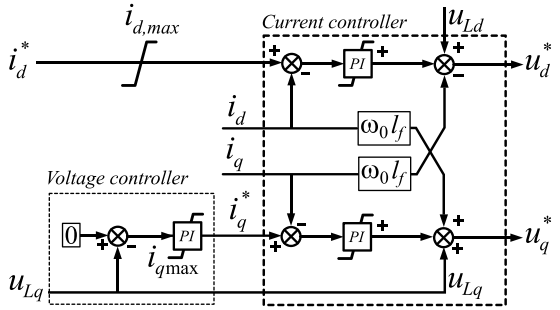

Fig. 5. Voltage and current control loops.

voltage vector is aligned along the internal reference frame, while the control of the voltage magnitude is achieved through the direct axis current that in turn is controlled through the current control loop shown in Fig. 5.

Then, neglecting the losses in the PV inverter, when the voltage vector is oriented along the d axis of the reference system ($u_{Lq} = 0$), the following relationship is met between the dc current and direct axis current component:

$$i_{dc} = \frac{3}{4} m_a i_d \tag{8}$$

where i_d is the direct component of the current vector and m_a is the amplitude modulation index. This means that the i_d current control outlined in Fig. 5 will demand the required dc current from the PV generator to maintain constant current at the ac side.

The effect of the voltage controller can be illustrated looking at the relation between current and voltage at the ac terminals of a single PV inverter which can be written as

$$i_d - i_{dg} = \frac{c}{\Omega_b} \frac{du_d}{dt} - cu_q \tag{9}$$

$$i_q - i_{qg} = \frac{c}{\Omega_b} \frac{du_q}{dt} - cu_d \tag{10}$$

As discussed in the system model in Section 2.2, by maintaining constant voltage, that is $\frac{du_d}{dt} = 0$, (note that in steady-state $u_q = 0$ and $u_d = u$), the active power supplied by the inverter is equal to the active power demanded by load. In the same manner, Eq. (10) states that by maintaining constant frequency (which is achieved by maintaining u_q constant or $\frac{du_q}{dt} = 0$), the reactive power supplied by the inverter is equal to the reactive power demanded by the load plus the reactive power supplied by the capacitive filter of the inverter.

On the other hand, at the PV generator, for the dc current drawn by the inverter, the PV generator will impose a certain dc voltage, following the I(V) characteristics of Fig. 3, i.e., for the dc current demanded by the inverter, the dc voltage will vary between the open-circuit voltage (at no-load) and the maximum power–voltage.

It has to be remarked that this voltage variation range is within the voltage variation admitted by the inverters (872 V and 700 V, respectively for the generator used in this paper). Therefore, the PV generator can supply any load up to the maximum power for the actual irradiance and temperature. The maximum power point represents the stability limit. When this point is reached a further dc current increase will reduce the PV generator power, as shown in Fig. 3. Consequently, the ac voltage controller of Fig. 4 will demand even more current, reducing even more the dc voltage and power. Eventually, the inverter will stop when the minimum operative dc voltage is reached. Obviously, the PV generator cannot supply any load over the maximum power for a given irradiance and temperature. To avoid this during the PSR after the black-out, the maximum power that the PV plant can supply can be estimated for the current irradiance and temperature and this constrain must be considered during the subsequent loading of the PV plant.

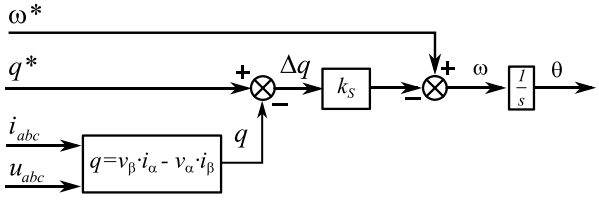

Fig. 6. Reactive Power Synchronization (RPS) loop.

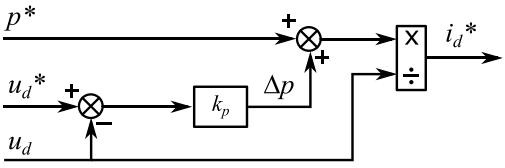

Fig. 7. Active Power Sharing (APS) control.

3.2. Reactive power synchronization

The Reactive Power Synchronization (RPS) block obtains the internal frequency, ω, for the control system as

$$\omega = \omega^* - (q^* - q)k_s \tag{11}$$

where ω^* is the frequency set-point, q^* is the reactive power set-point and k_s is the droop gain. This relation is represented in the block diagram of Fig. 6.

In contrast with conventional solutions in which frequency is proportional to active power, here the internal frequency ω changes proportionally to the reactive power supplied by the PV inverter. Therefore, the synchronism does not depend on the variations in active power due to variations in the available PV power (e.g. irradiance or temperature variations) or in the load power.

Also, the use of a Phased-Locked Loop (PLL) is avoided. The reference angle for the calculation of the dq components is obtained from the integration of the internal frequency ω given by (11) while the VCC ensures that $u_{Lq} = 0$ and thus that the voltage vector is aligned with the reference axis.

3.3. Active power sharing

As shown in Eq. (9), the balance between generation and load active powers is obtained through the regulation of the voltage magnitude.

In a single PV generator case, the active power needed to supply the demanded load can be obtained by controlling the ac voltage magnitude by means of a PI controller. However, in the two PV generators case operating in parallel, the load demand must be shared between them. For this purpose, an Active Power Sharing (APS) control is implemented as given in Fig. 7. Thus, the active current reference $i_d{}^*$ is obtained from the power–voltage droop control law where $u_d{}^*$ is the voltage set-point, p^* is the active power set-point and k_p is the droop gain.

$$u_d \cdot i_d{}^* = p^* - (u_d{}^* - u_d)k_p \tag{12}$$

Given this control law, each inverter supplies the same load, provided that they are connected to the same bus, with a given voltage deviation that depends on the inverters loading. Note that if by any reason, equally sharing of the load is not desired, a different control gain k_p can be used in each inverter.

If $i_d{}^*$ cannot be achieved at one generator, voltage will decrease and the other generator i_d will increase automatically. A new stable operating point will be reached at a different voltage. Therefore, two generators can operate in parallel even if the $i_d{}^*$ provided by (12) cannot be achieved by one of them.

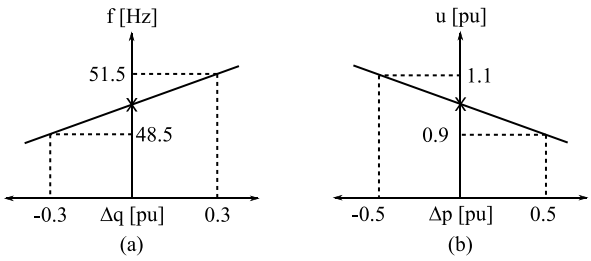

Fig. 8. Representation of droop gain tuning effect.

Note that if a conventional P/f droop was used for synchronization and active power sharing, if one of the generators cannot fulfil a given $i_d{}^*$ value, due to a lower irradiance, that unit would lose the synchronism. In contrast, this paper uses reactive power for synchronization which does not depend on resource availability.

The droop gains k_s and k_p should be selected considering the desired operation range. In steady state, the frequency and voltage vary following changes in the load demand. So, if the load demand is equal to the settings (i.e: q^* and p^*), the system will be operating at nominal frequency and voltage. Only when load demand deviates from settings, a change in voltage and frequency is produced, proportional to the active and reactive power variation respectively. This is represented graphically on Fig. 8 for $k_p = 5$ and $k_s = 0.1$. Voltage and frequency are kept within admissible ranges, considering that the expected load variations are within ±0.3 pu for reactive power (which represents a 0.9 power factor at full load) and ±0.5 pu for active power variation around 0.5 pu power setting (which covers the full operation range from 0 to 1 pu).

Therefore, k_s and k_p are parameters that have to be tuned according to the expected load variation and maximum allowable voltage and frequency variations so different values could be selected depending on the islanded system. Note that secondary regulation loops could also be included as in traditional power systems [31] or hierarchical microgrids [32], to maintain nominal voltage and frequency by modifying the reference settings.

4. Stability analysis

This section demonstrates the stability of the proposed solution. For this purpose, the small-signal analysis of the linearized model, presented in previous sections, is performed. The system parameters are given in Table 3.

The model states include the converter current and PCC voltage dq components (defined in Eqs. (4)–(7)) as well as the internal states of the VCC of Fig. 5 and the phase displacement between the converter voltage u and the PCC voltage u_L, also known as power angle.

The power angle δ is obtained from the difference between the internal frequency given by Eq. (11), ω, and the grid frequency, ω_g, as

$$\frac{1}{\Omega_b}\frac{d\delta}{dt} = \omega - \omega_g \tag{13}$$

Regarding the internal states of the VCC, from Fig. 5 the modulating voltage reference u^* is calculated as

$$u_d{}^* = k_{pc}(i_d^* - i_d) + k_{ic}x_{dc} - \omega_0 l_f i_q \tag{14}$$

$$u_q{}^* = k_{pc}(i_q^* - i_q) + k_{ic}x_{qc} + \omega_0 l_f i_d, \tag{15}$$

where x_{dc} and x_{qc} are the d-q current error states and k_{pc} and k_{ic} are the proportional and integral gains of the current controllers, respectively. The current controllers error states are defined as

$$\frac{1}{\Omega_b}\frac{dx_{dc}}{dt} = i_d^* - i_d \tag{16}$$

Table 3
Base case system parameters in pu.

Label	Value	Units	Description
l_{f1}, l_{f2}	0.2	pu	Filter inductance
r_{f1}, r_{f2}	0.004	pu	Filter resistance
c_1, c_2	0.05	pu	Total ac capacitance
l_g	0.1	pu	Grid inductance
r_g	0.002	pu	Grid resistance
c_{dc}	0.35	pu	Total dc capacitance
k_{pc1}, k_{pc2}	2	pu	VCC current proportional gain
k_{ic1}, k_{ic2}	0.637	pu	VCC current integral gain
k_{pv1}, k_{pv2}	2.5	pu	VCC voltage proportional gain
k_{iv1}, k_{iv2}	0.127	pu	VCC voltage integral gain
k_{s1}, k_{s2}	0.1	pu	RPS loop gain
k_{p1}, k_{p2}	2.5	pu	APS loop gain
ω_0	1	pu	Frequency parameter for VCC cross-coupling
$Ts, cont$	200	µs	Control sampling time
$Ts, power$	10	µs	Power circuit sampling time

Table 4
Base-case eigenvalue analysis.

λ_i	Eigenvalues [rad/s]	Frequency [Hz]	Damping ratio [pu]	Dominant states
1 – 2	−490.6 ± 10 870.8i	1730.1	0.045	u_{Lq}, i_q
3 – 4	−6.1 ± 4433.0i	705.5	0.001	u_{Ld}, i_d
5	−1348.8	0	1	i_d
6	−459.1	0	1	x_{vq}, i_q
7 – 8	−70.3 ± 208.4i	33.16	0.32	δ, i_q
9	−10.5	0	1	x_{vq}, x_{cq}
10	−233.7	0	1	x_{cd}

$$\frac{1}{\Omega_b}\frac{dx_{qc}}{dt} = i_q^* - i_q \tag{17}$$

The quadrature component of the current reference, i_q^*, is obtained from the regulation of the quadrature component of the voltage, u_{Lq}, as

$$i_q^* = -k_{pv}u_{Lq} + k_{iv}x_{qv}, \tag{18}$$

where k_{pv} and k_{pv} are the proportional and integral gains of the voltage controller, respectively. As in the current controller, x_{qv} is the q voltage error state, given by:

$$\frac{1}{\Omega_b}\frac{dx_{qv}}{dt} = -u_{Lq} \tag{19}$$

The set of Eqs. (4)–(7), (13), (16), (17) and (19) define the modelled state space system. The resulting eigenvalues are given in Table 4, including their frequency and damping ratio. The participation of the states in each mode is given by the participation factors. Dominant states in each mode are also given in Table 4. The stability of the system is demonstrated since all the eigenvalues have negative real parts.

5. Results and discussions

In this section the proposed control system is validated using the case study shown in Fig. 1. The results presented here have been obtained using a detailed switching model of the system in a co-simulation between MATLAB/Simulink and PSIM, implementing the control system and the system power components, respectively. Loads are modelled as constant impedances. The parameters used in the simulation are given in Table 1, Tables 2 and 3. The results have also been validated with a reduced scale experimental set-up.

Results have been obtained in a single run in which different testing events are applied sequentially. For the sake of clarity, the test results have been divided into multiple figures that highlight the different events. Tests are intended to represent the complete black-start process using a PV plant, from the starting point in which an isolated system is energized to the connection to the main grid to contribute to the PSR.

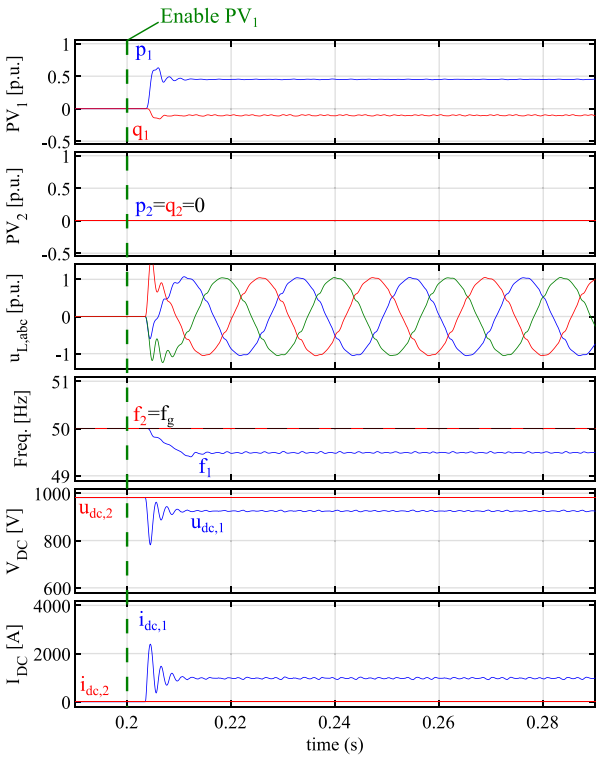

Fig. 9. Results for the black-start start-up of PV_1 (t=0.2 s).

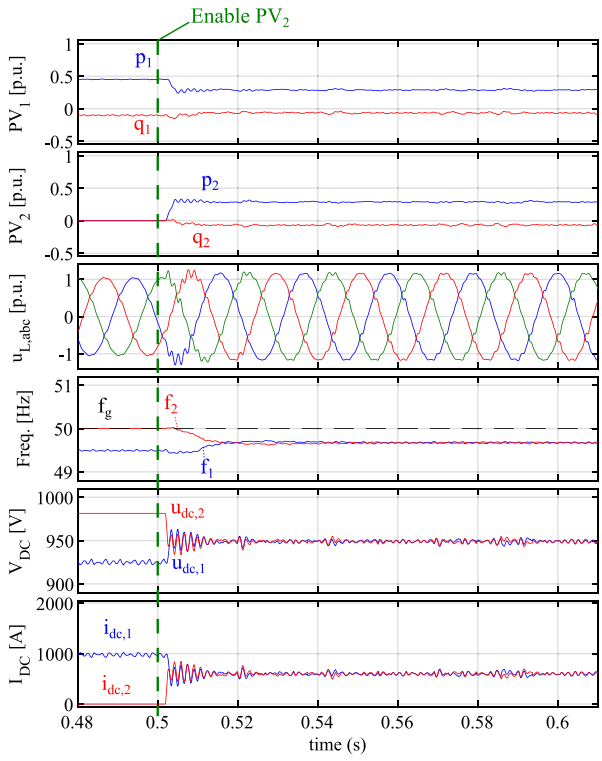

Fig. 10. Results for the connection of PV_2 (t=0.55 s).

The first event is the connection of one of the PV generators (PV_1) as shown in Fig. 9. The connection is managed by enabling the PV inverter control. Before the converter is enabled, the PV generator is operating in open circuit with a dc voltage determined by the P(V) characteristics at the given irradiance and temperature (V_{dc} = 872 V at 1000 W/m^2, 20 °C).

Once the VSC is enabled (t=0.2 s), the converter starts generating the ac voltage, supplying the active and reactive demanded by the local loads, established at a value of $p_1 = 0.5$ pu and $q_1 = -0.1$ pu. This in turn leads to a variation in the PV generator dc voltage and current to the required level to maintain power balance. The proposed control system ensures the balance between the PV_1 generation and the load, by automatically increasing dc current and reducing dc voltage.

The system frequency and voltage magnitude will be established as a result of the control law given by Eqs. (11) and (12) for the RPS control and the APS control, respectively. Frequency results are not measured but obtained from each RPS controls (ω in Fig. 6). A low pass filter has been used to reduce noise in the frequency signals visualization. The RPS control is set-up to obtain nominal frequency at q=0 pu, while the APS control is set-up to obtain nominal voltage at p=0.5 pu. As a result, there is a frequency drop, when the converter is connected and starts supplying reactive power to the load. On the other hand, voltage is established at a magnitude value over nominal, following the voltage–power characteristic of Fig. 7.

Once the PV_1 is enabled and supplying the load, PV_2 is connected. This process has been done sequentially just to show the synchronizing capability, although both converters could start independently and then synchronized before starting to supply the load. Due to the distributed control structure, there is not a "master" unit that needs to be connected first.

The results of the connection of PV_2 are shown in Fig. 10. The PV inverter is enabled at t=0.5 s. For the connection, first, it is checked that the internal voltage angle is close to the measured PCC voltage angle. This difference is evaluated using the value of u_{Lq}.

Both inverters are then synchronized, operating at the same frequency, given by the reactive power loading of each inverter, sharing the reactive power demand, following the RPS control law. Moreover, following the APS control law, both inverters also share the active power demand, so in Fig. 10, PV_1 reduces its output by half, while PV_2 increases its output to the same value. In this case, both controllers have been designed for the converters to contribute equally to the load supply, although the controllers can be set for any contribution proportion by using different gains k_s and k_p in each converter. So the final operating point of both converters leads to around $p_1 = 0.25$ pu and $q_1 = -0.05$ pu.

The change in active and reactive power leads to a change in the frequency and voltage of the system. Note that nominal frequency can be obtained for any reactive demand if a secondary control loop is added. This control loop would set the required frequency reference signal ω^* so that the actual frequency is equal to the desired frequency (e.g. 50 Hz).

Fig. 10 also shows the response of the PV generators. As already stated, when PV_2 is connected the load is shared between both generators. At the dc side, PV_1 reduces its load and as a result dc voltage increases and dc current decreases. While PV_2, that was initially operating at no load, increases its load by reducing dc voltage and increasing dc current. At the final operating point, both PV generators operate with the same dc voltage and current.

During the energization of the islanded system, as part of the black start procedure, generators are subjected to load variations, as a consequence of new loads being added to the system. A load variation is then introduced in the test at t=0.7 s. An additional constant impedance load is connected, increasing the total power demand. The results are shown in Fig. 11. The control responds increasing the generation from the PV generators. The new demand is supplied equally by both inverters. As a consequence of the load increase, there is a voltage drop, following the APS control law. Due to the change in voltage at the PV inverters filter capacitor, there is a variation of reactive power demand (around 0.03 pu). Therefore, the relation between reactive power and frequency

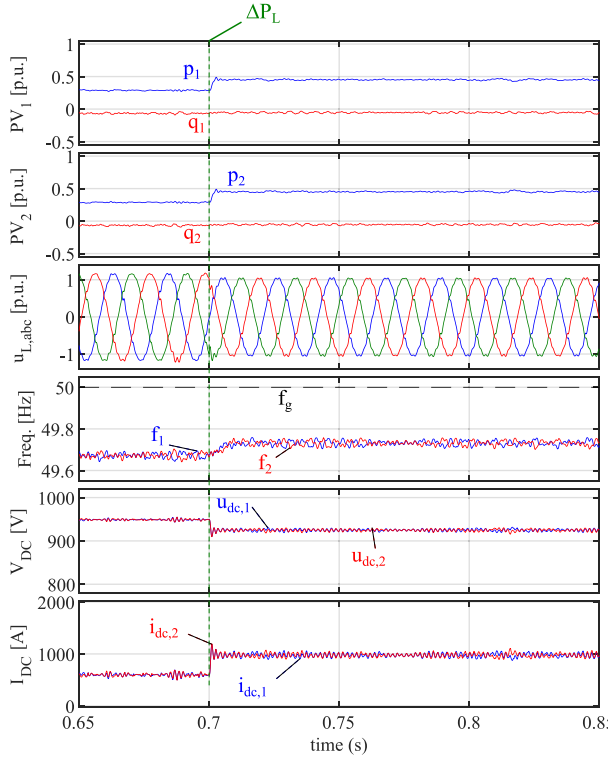

Fig. 11. Results for a variation in the local load (t=0.7 s).

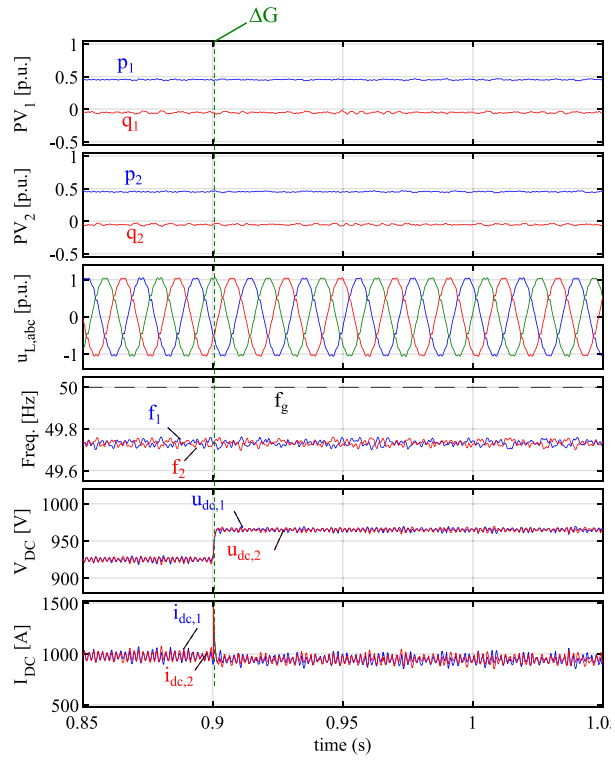

Fig. 13. Results for a variation in irradiance (t=0.9 s).

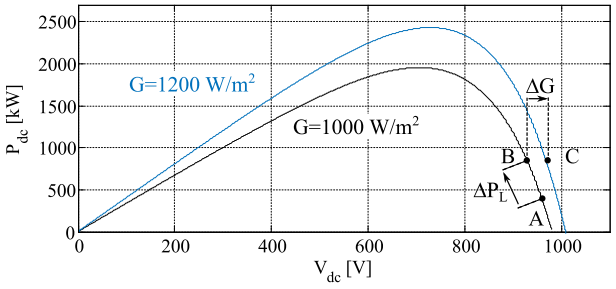

Fig. 12. Changes in the operating point of PV_1 generator under load increment (A to B) and irradiance increment (B to C).

introduced by the RPS, produces a frequency variation (around 0.003 pu or 0.15 Hz).

Moreover, due to the load change, there is a variation in the dc voltage and current. This change in the PV generator operating point is represented in Fig. 12, where point A represents the operating point previous to the load increment and B represents the operating point after the load increment.

To further demonstrate the black-start capability, a variation in the solar irradiance, from G=1000 W/m^2 to G=1200 W/m^2, is introduced at t=0.9 s. Note that although solar irradiation changes slowly during the day, a step has been applied here to demonstrate the dynamic capability of the proposed control system under such disturbance. In this case, load remains constant at the value of the previous test, so the active and reactive power operating points do not change. However, the PV generators operating points change since the PV characteristic has changed. This change is represented in Fig. 12, where point C represents the new operating point after the irradiance variation. The dc voltage and current change providing the same power at a different operating point, as shown in Fig. 13.

Finally, in order to test the capability of the system to switch from isolated to grid-tied mode, the isolated system is connected to the main grid by closing SW_g of Fig. 1 at t=1.1 s. Results, given in Fig. 14, shows that both converters synchronize automatically, without having to switch the control from isolated to grid-tied mode. Now they follow the grid frequency, and as a result they follow the reactive power command, as given by the RPS control law. Synchronization control for the closing of the switch has not been implemented, as the purpose is to demonstrate the ability of the proposed control system to maintain synchronism when switching from isolated to grid-tied mode, even when the switch is closed without meeting the synchronism conditions. This explains the high disturbance in the converters frequency immediately after the switch is closed.

On the other hand, the voltage magnitude is also imposed by the grid, so the APS control will follow the active power command in Fig. 7. Therefore, grid connection produces a reduction on the generated power as the power reference was lower than the islanded load, and the dc voltage and current are automatically adjusted to this new power value. Nevertheless, once the converters are synchronized to the grid, dc power control can be established by a MPPT controller. This part has not been included in the simulation, as it is the well-know PV plant operation mode.

The presented simulations have been further validated using a reduced-scale (10 kW) experimental set-up. The set-up is based on the connection of two inverters in an isolated environment in which each inverter has a controllable DC-source connected to its DC terminals and both inverters are connected the same AC load. A controllable DC-source has been programmed to emulate the PV plant, so the PV plant Voltage–Current curve provides a DC current depending on the DC voltage at its terminals. The Voltage–Current curve implemented is the one shown in Fig. 3. A scheme of this experimental set-up is shown in Fig. 15

Only the isolated operation is reproduced. Fig. 16 shows the results obtained with the experimental set-up. As in the simulation case, a load step is introduced during the isolated operation. Only the measurements corresponding to one of the inverters is shown. It can be

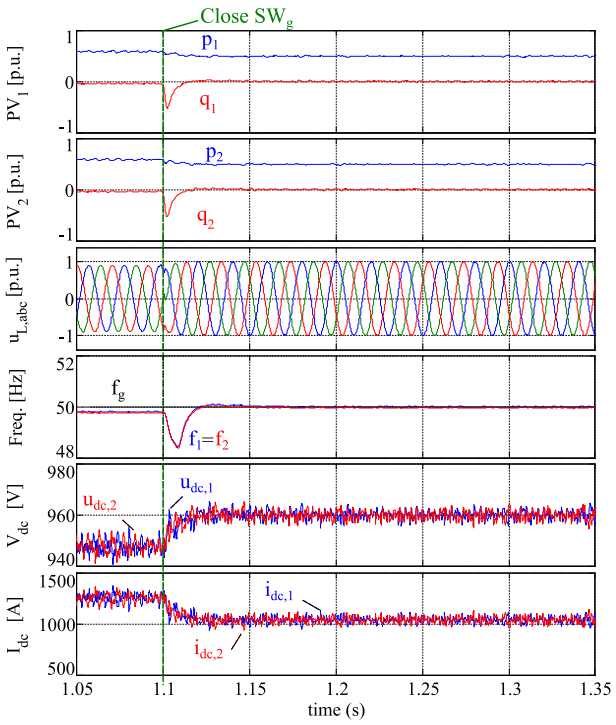

Fig. 14. Results for the connection to the main grid (t=1.1 s).

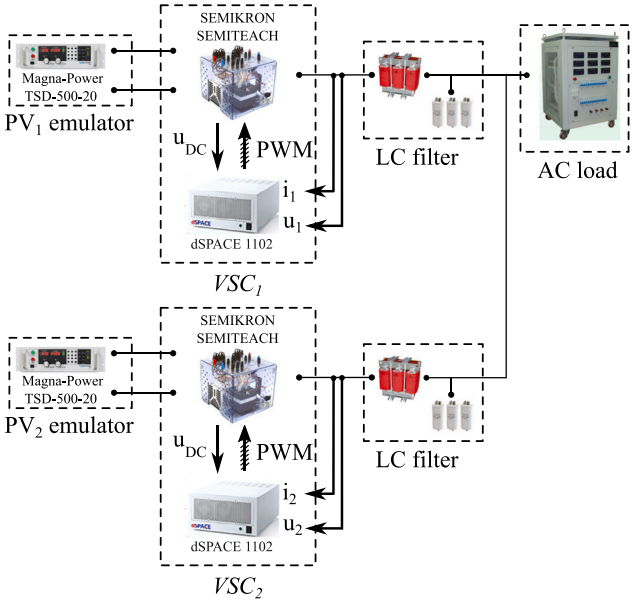

Fig. 15. Scheme of the reduced scale experimental test-bench.

observed that the experimental results matches the results obtained in simulations (see Fig. 11). As a result of the load step, the active and reactive power change and also the DC voltage and current, to match the load power. However, the change in DC voltage and current is slower than in the simulations due to the dynamics of the controllable DC sources.

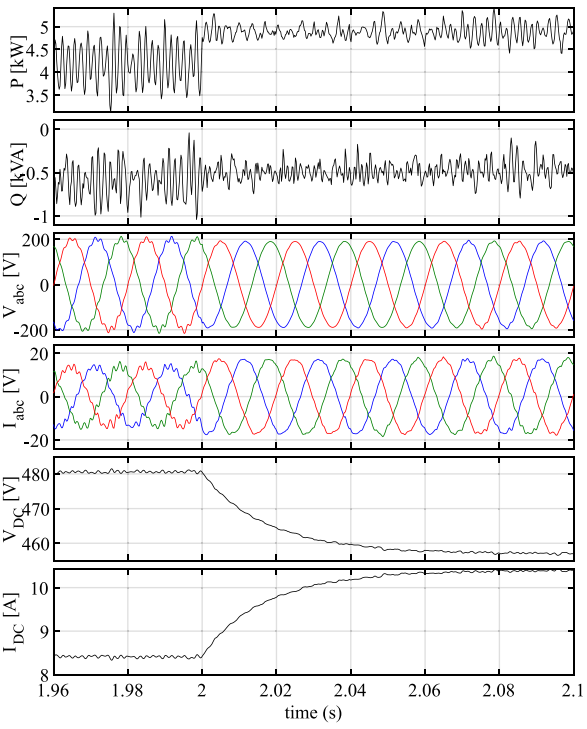

Fig. 16. Results for the reduced scale experimental test-bench.

6. Conclusions

This paper proposes a control system to allow photovoltaic (PV) power plants to accomplish a black-start process autonomously, without requiring additional units such as energy storage systems or synchronous generators. This control could be used to enable the participation of PV generators on the Power System Restoration (PSR).

With the proposed control system, each PV generator is able to regulate the voltage and frequency of the PV power plant, when operating in islanded mode. The proposed solution ensures any additional PV generator can operate in synchronism and also that the generators can operate in synchronism with the grid, once it is reestablished.

The PV generators supply the power demanded by the load and share this load equally. In each generator, the dc power that match the load is met by automatically adjusting the required dc voltage and current, in contrast with conventional Maximum Power Point Tracking (MPPT) algorithms that seek to extract the maximum available power.

A comprehensive model of the proposed control system is presented and its stability has been demonstrated using the small-signal stability analysis. To validate the proposal, a case study of a PV plant that performs a full black-start process has been employed. The PV plant for the case study is composed of two independent PV generators connected in parallel and the case study includes the analysis of islanding operation and grid-tied operation.

Results demonstrate that the proposed control system is able to provide the expected functionalities during a black-start process. When the grid is not available, the PV generators are able to perform an autonomous starting and synchronize to each other. This has been demonstrated both with experimental and simulation results. The generation and demand are balanced even during load or irradiance variations. When the grid is reestablished, it is possible to perform a hot-swap to grid connected mode so the PV power plant can support the system during the PSR process. However, hot-swapping has not been tested in the experimental set-up. It is expected to perform these tests in the future.

CRediT authorship contribution statement

Andrés Peña Asensio: Conception and design of study, Analysis and/or interpretation of data, Writing – original draft, Writing – review & editing. **Santiago Arnaltes Gómez:** Conception and design of study, Analysis and/or interpretation of data, Writing – original draft, Writing – review & editing. **Jose Luis Rodriguez-Amenedo:** Conception and design of study, Analysis and/or interpretation of data, Writing – original draft, Writing – review & editing.

Declaration of competing interest

The authors declare that they have no known competing financial interests or personal relationships that could have appeared to influence the work reported in this paper.

Data availability

Data will be made available on request.

Acknowledgements

This paper was supported by the Spanish Research Agency under project reference PID2019-106028RB-I00/AEI/10.13039/501100011033. All authors approved version of the manuscript to be published

References

[1] Liu Y, Fan R, Terzija V. Power system restoration: a literature review from 2006 to 2016. J Mod Power Syst Clean Energy 2016;4(3):332–41. http://dx.doi.org/10.1007/s40565-016-0219-2, URL http://link.springer.com/10.1007/s40565-016-0219-2.

[2] Kroposki B, Johnson B, Zhang Y, Gevorgian V, Denholm P, Hodge BM, Hannegan B. Achieving a 100% renewable grid: Operating electric power systems with extremely high levels of variable renewable energy. IEEE Power Energy Mag 2017;15(2):61–73. http://dx.doi.org/10.1109/MPE.2016.2637122.

[3] Li J, You H, Qi J, Kong M, Zhang S, Zhang H. Stratified optimization strategy used for restoration with photovoltaic-battery energy storage systems as black-start resources. IEEE Access 2019;7:127339–52. http://dx.doi.org/10.1109/ACCESS.2019.2937833.

[4] Xu Z, Yang P, Zeng Z, Peng J, Zhao Z. Black start strategy for pv-ess multi-microgrids with three-phase/single-phase architecture. Energies 2016;9(5):372. http://dx.doi.org/10.3390/en9050372,.

[5] Thale S, Agarwal V. A smart control strategy for the black start of a microgrid based on PV and other auxiliary sources under islanded condition. In: Conference record of the IEEE photovoltaic specialists conference. 2011, p. 002454–9. http://dx.doi.org/10.1109/PVSC.2011.6186443.

[6] Yu L, Lei J, Guo X, Yang P, Zeng Z, Xu Z, Zheng Q. Study on black start strategy of multi-microgrids with PV and energy storage systems considering general situations. In: 2015 6th international conference on power electronics systems and applications: electric transportation - automotive, vessel and aircraft, PESA 2015. Institute of Electrical and Electronics Engineers Inc.; 2016, http://dx.doi.org/10.1109/PESA.2015.7398888.

[7] Zhang Y, Zhao L, Miao M, Li J, Shi T. Modelling and control strategy for hybrid PV and central receiver CSP in power system restoration. China Int Conf Electr Distribution, CICED 2018;2109–13. http://dx.doi.org/10.1109/CICED.2018.8592112.

[8] Perez E, Beltran H, Aparicio N, Rodriguez P. Predictive power control for PV plants with energy storage. IEEE Trans Sustain Energy 2013;4(2):482–90. http://dx.doi.org/10.1109/TSTE.2012.2210255.

[9] Krommydas KF, Alexandridis AT. Modular control design and stability analysis of isolated PV-source/battery-storage distributed generation systems. IEEE J Emerg Sel Top Circuits Syst 2015;5(3):372–82. http://dx.doi.org/10.1109/JETCAS.2015.2462172.

[10] Chandorkar MC, Divan DM, Adapa R. Control of parallel connected inverters in standalone ac supply systems. IEEE Trans Ind Appl 1993;29(1):136–43. http://dx.doi.org/10.1109/28.195899.

[11] Marwali M, Keyhani a. Control of distributed generation systems-Part I: Voltages and currents control. IEEE Trans Power Electron 2004;19(6):1541–50. http://dx.doi.org/10.1109/TPEL.2004.836685, URL http://ieeexplore.ieee.org/abstract/document/1353345/.

[12] De Brabandere K, Bolsens B, Van den Keybus J, Woyte A, Driesen J, Belmans R. A voltage and frequency droop control method for parallel inverters. IEEE Trans Power Electron 2007;22(4):1107–15. http://dx.doi.org/10.1109/TPEL.2007.900456, URL http://ieeexplore.ieee.org/document/4267747/.

[13] Guerrero JM, Chandorkar M, Lee TL, Loh PC. Advanced control architectures for intelligent microgrids. Part I : Decentralized and hierarchical control. IEEE Trans Ind Electron 2013;60(4):1254–62. http://dx.doi.org/10.1109/TIE.2012.2194969, arXiv:arXiv:1011.1669v3.

[14] Zhong QC. Robust droop controller for accurate proportional load sharing among inverters operated in parallel. IEEE Trans Ind Electron 2013;60(4):1281–90. http://dx.doi.org/10.1109/TIE.2011.2146221, URL http://ieeexplore.ieee.org/abstract/document/5754579/.

[15] Amenedo JLR, Gomez SA, Alonso-Martinez J, De Armas MG. Grid-forming converters control based on the reactive power synchronization method for renewable power plants. IEEE Access 2021;9:67989–8007. http://dx.doi.org/10.1109/ACCESS.2021.3078078.

[16] Sun X, Wu W, Li X, Zhao Q. A research on photovoltaic energy controlling system with maximum power point tracking. Proc Power Convers Conf-Osaka 2002, PCC-Osaka 2002 2002;2:822–6. http://dx.doi.org/10.1109/PCC.2002.997626, URL https://ieeexplore.ieee.org/abstract/document/997626/.

[17] Safari A, Mekhilef S. Simulation and hardware implementation of incremental conductance MPPT with direct control method using cuk converter. IEEE Trans Ind Electron 2011;58(4):1154–61. http://dx.doi.org/10.1109/TIE.2010.2048834.

[18] Kish G, Lee J, Lehn P. Modelling and control of photovoltaic panels utilising the incremental conductance method for maximum power point tracking. IET Renew Power Gener 2012;6(4):259–66. http://dx.doi.org/10.1049/iet-rpg.2011.0052, URL https://ieeexplore.ieee.org/document/6291074/.

[19] Wu W, Pongratananukul N, Qiu W, Rustom K, Kasparis T, Batarseh I. DSP-based multiple peak power tracking for expandable power system. Conf Proc IEEE Appl Power Electron Conf Exposition APEC 2003;1:525–30. http://dx.doi.org/10.1109/apec.2003.1179263.

[20] Subudhi B, Pradhan R. A comparative study on maximum power point tracking techniques for photovoltaic power systems. IEEE Trans Sustain Energy 2013;4(1):89–98. http://dx.doi.org/10.1109/TSTE.2012.2202294.

[21] Hussein K, Muta I, Hoshino T, Osakada M. Maximum photovoltaic power tracking: an algorithm for rapidly changing atmospheric conditions. IEE Proc Gener Transm Distrib 1995;142(1):59–64. http://dx.doi.org/10.1049/ip-gtd:19951577, URL https://digital-library.theiet.org/content/journals/10.1049/ip-gtd_19951577.

[22] Syafaruddin, Karatepe E, Hiyama T. Artificial neural network-polar coordinated fuzzy controller based maximum power point tracking control under partially shaded conditions. IET Renew Power Gener 2009;3(2):239–53. http://dx.doi.org/10.1049/iet-rpg:20080065, URL https://digital-library.theiet.org/content/journals/10.1049/iet-rpg_20080065.

[23] Yazdani A, Di Fazio AR, Ghoddami H, Russo M, Kazerani M, Jatskevich J, Strunz K, Leva S, Martinez JA. Modeling guidelines and a benchmark for power system simulation studies of three-phase single-stage photovoltaic systems. IEEE Trans Power Deliv 2011;26(2):1247–64. http://dx.doi.org/10.1109/TPWRD.2010.2084599.

[24] Feldmann D, de Oliveira RV. Operational and control approach for PV power plants to provide inertial response and primary frequency control support to power system black-start. Int J Electr Power Energy Syst 2021;127(April 2020):106645. http://dx.doi.org/10.1016/j.ijepes.2020.106645.

[25] Liu J, Miura Y, Ise T. Comparison of dynamic characteristics between virtual synchronous generator and droop control in inverter-based distributed generators. IEEE Trans Power Electron 2016;31(5):3600–11. http://dx.doi.org/10.1109/TPEL.2015.2465852.

[26] D'Arco S, Suul JA. Equivalence of virtual synchronous machines and frequency-droops for converter-based Microgrids. IEEE Trans Smart Grid 2014;5(1):394–5. http://dx.doi.org/10.1109/TSG.2013.2288000.

[27] Pena Asensio A, Arnaltes S, Rodriguez-Amenedo JL, Cardiel-Alvarez MA. Reactive power synchronization method for voltage sourced converters. IEEE Trans Sustain Energy 2019;10(3). http://dx.doi.org/10.1109/tste.2019.2911453, 1–1.

[28] Pena Asensio A, Arnaltes S, Rodriguez-Amenedo JL, Cardiel-Alvarez MA. Decentralized frequency control for black start of full-converter wind turbines. IEEE Trans Energy Convers 2020. http://dx.doi.org/10.1109/TEC.2020.3011611, 1–1.

[29] Guerrero JM, Vasquez JC, Matas J, de Vicuna LG, Castilla M. Hierarchical control of droop-controlled AC and DC MicrogridsA general approach toward standardization. IEEE Trans Ind Electron 2011;58(1):158–72. http://dx.doi.org/10.1109/TIE.2010.2066534, URL http://ieeexplore.ieee.org/lpdocs/epic03/wrapper.htm?arnumber=5546958.

[30] Amirnaser Y, Reza I. Voltage-sourced converters in power systems : modeling, control, and applications. John Wiley & Sons; 2010, p. 541.

[31] Prabha Kundur MGL, Balu NJ. Power system stability and control. vol. 7, McGraw-hill New York; 1994, URL http://www.academia.edu/download/28284657/invitation.pdf.

[32] Palizban O, Kauhaniemi K, Guerrero JM. Microgrids in active network management - Part I: Hierarchical control, energy storage, virtual power plants, and market participation. Renew Sustain Energy Rev 2014;36:428–39. http://dx.doi.org/10.1016/j.rser.2014.01.016.